Nonlinear Response of Grafted Semiflexible Polymers in Shear Flow

Yong Woon Kim,*,†,‡ V. Lobaskin,§ C. Gutsche,|| F. Kremer,|| Philip Pincus,‡ and Roland R. Netz§

School of Physics, Korea Institute for Advanced Study, Seoul 130-722, Korea; Materials Research Laboratory, University of California at Santa Barbara, Santa Barbara, California 93106; Physics Department, Technical University Munich, 85748 Garching, Germany; and Institut für Experimentelle Physik I der Universität Leipzig, 04103 Leipzig, Germany

Received January 28, 2009; Revised Manuscript Received March 31, 2009

ABSTRACT: Using Brownian-hydrodynamic and lattice-Boltzmann simulations, we study the nonlinear response of grafted semiflexible polymers to shear flow as a function of shear rate, grafting density, and chain stiffness. Simulation results for brush height and flow stagnation layer height agree well with a mean-field theory that incorporates the interplay of hydrodynamic screening and drag-induced polymer deformation. Our predictions for the stagnation height show excellent agreement with recent experiments on the nonlinear hydrodynamic drag of DNA-grafted colloids held in a laser trap.

The nonequilibrium behavior of polymers tethered to surfaces has lately moved into the focus of attention. Of particular interest are grafted polymer layers in shear flow which is a scenario related to various applications encompassing stabilization of colloidal dispersions[1] or biocompatible lubricants.[2] Understanding of the rheological response of this system is crucial for a number of nanofluidic devices involving end-tethered polymers. Examples include controlled fluid pumping using anchored linear appendices,[3] biomolecular sorting and filtration through laboratory-on-a-chip devices,[4] and smart flow gating through polymer-grafted nanopores.[5] Sheared polymer brushes have thus been extensively studied via experimental,[6,7] analytical,[8−10] and numerical methods.[11−16] In order to understand the significant increase of normal forces between polymer brushes under oscillatory shear,[6] previous work has focused on shear effects on the brush height, i.e., swelling or collapse of brushes.[9−12,14−16] On the biological side, terminally attached polymers in shear are encountered in the glycocalix in the bloodstream, which forms an essential barrier for infection and transport of nanoparticles from the bloodstream to the vessel cells.[17] Similar structures are encountered in mucus layers such as the lung surface[18] and the mucus-like interior of nuclear pores.[19]

As any object that is held stationary in external flow, a brush screens the shear flow by opposing hydrodynamic drag forces and thereby modifies the flow profile. Since a polymer is elastic and thus reacts to drag forces by a shape deformation that depends on the shear rate, the screening of the boundary flow depends via the polymer deformation on the shear rate applied. This leads to a nonlinear boundary condition in the otherwise linear Stokes flow that manifests itself already at experimentally accessible and rather modest shear rates. Experimentally most relevant is the stagnation height, i.e., the height of the layer at which the velocity of the linearly extrapolated bulk shear flow reaches zero. The stagnation height determines the hydrodynamic friction force between laterally sheared opposing brushes, and it plays an important role in the rheology of polymer-coated colloids and surfaces, i.e., in regulating the interfacial hydrodynamic properties of a variety of systems. However, a comprehensive picture of the hydrodynamic response of grafted polymer layers and in particular of the stagnation length to applied shear is yet lacking.

Stiff biopolymers such as DNA have recently received considerable attention as modulators of surface activity in a variety of practical applications. Semiflexible (or wormlike) polymers usually exhibit static and dynamic behavior that on small scales is remarkably distinct from flexible polymers.[20] From a fundamental viewpoint, it is therefore valuable to explore how semiflexible polymer brushes respond to applied shear flow and how the effect of finite persistence length of chains comes into play. Previous theoretical studies have considered mostly dense brushes composed of flexible polymers, and theoretical work on the shear response of grafted wormlike chains is not available. In this work, we present a systematic study of the stagnation length and the brush height of a layer of grafted semiflexible chains as a function of shear rate, grafting density, and bending rigidity. To this end, we perform extensive Brownian-hydrodynamic (BD) and lattice-Boltzmann (LB) simulations in the global parameter space, explicitly incorporating hydrodynamic interactions between the polymers, the presence of a no-slip surface, and the polymer-conformation-dependent screening of the flow profile. BD simulations are advantageous for dilute polymer systems since the numerical effort only depends on the number of polymer beads (and not the system volume), LB simulation times scale with the system volume, and thus LB becomes efficient at high polymer concentrations. It is therefore of great methodological interest to quantitatively compare both methods at intermediate concentrations where they both are applicable. We also develop a hydrodynamic mean-field theory that explicitly incorporates the coupling between flow stagnation and chain deformation by laterally averaging the flow profile (on a mean field level) and by only considering the most dominant (that is ground-state) chain conformation. It is found that the theory agrees well with numerical results and can be applied at very low shear rates where both simulation techniques have efficiency problems. Our theoretical predictions explain the pronounced nonlinear dependence of the effective hydrodynamic radius of a DNA-grafted colloid on the laminar solvent velocity that was found in recent laser trap experiments.[21]

* To whom correspondence should be addressed.
† Korea Institute for Advanced Study.
‡ University of California at Santa Barbara.
§ Technical University Munich.
|| Institut für Experimentelle Physik I der Universität Leipzig.

10.1021/ma900184e CCC: $40.75
Published on Web 05/01/2009

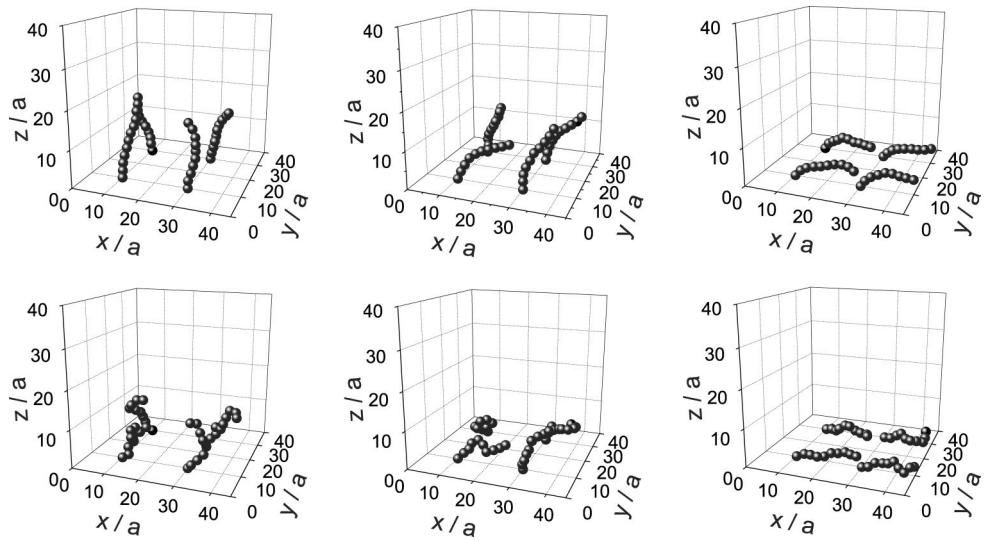

Figure 1. BD snapshots of sheared semiflexible polymers with different persistence lengths (bottom row: $l_p/l = 0.2$; top row: $l_p/l = 10$) at grafting density $\rho = 1$. To the left no shear flow is applied, in the middle column the shear rate is $\tilde{\dot{\gamma}} = l^3\eta\dot{\gamma}/k_BT = 24$ and to the right $\tilde{\dot{\gamma}} = 240$.

The anchored semiflexible polymers are modeled as N connected spherical monomers of radius a subject to the elastic energy of a discretized wormlike chain $V = \sum_{i=0}^{N-1}[(\gamma/4a)(r_{ii+1} - 2a)^2 + (\kappa/2a)(1 - \cos\theta_i)]$, where θ_i is the angle between neighboring bonds, κ and γ denote the bending and stretching moduli, and $\kappa/\gamma = a^2/4$ for an isotropic elastic rod.[22] The persistence length is $l_p = \kappa/k_BT$, and the length of an unstretched chain is $l = 2aN$. Mutual overlap of monomers is prevented by a truncated Lennard-Jones potential, and the polymers are oriented vertically to the surface at their grafted base.

The Brownian-hydrodynamic simulations are based on the Langevin equation

$$\dot{\mathbf{r}}_i(t) = -\sum_j \boldsymbol{\mu}_{ij}(\mathbf{r}_i, \mathbf{r}_j)\nabla_{\mathbf{r}_j}V + \mathbf{u}_\infty(\mathbf{r}_i) + \boldsymbol{\xi}_i \qquad (1)$$

The external bare shear profile, $\mathbf{u}_\infty(\mathbf{r}) = \dot{\gamma}z\hat{\mathbf{x}}$ with shear rate $\dot{\gamma}$, is modified by the presence of the polymer. We rescale all lengths and energies and express the dimensionless shear rate by $\tilde{\dot{\gamma}} = l^3\dot{\eta}\gamma/k_BT$, where η is the solvent viscosity. Full hydrodynamic interactions are taken into account via the nondiagonal mobility tensor $\boldsymbol{\mu}_{ij}$ on the Rotne−Prager level which correctly accounts for the no-slip wall at position $z = 0$.[23] The random forces are correlated to each other according to $\langle\xi_i^\alpha(t)\xi_j^\beta(t')\rangle = 2k_BT\mu_{ij}^{\alpha\beta}(\mathbf{r}_i,\mathbf{r}_j)\delta(t - t')$ where the self-mobility is constant and given by $\mu_{ii}^{\alpha\beta} = \delta_{\alpha\beta}/6\pi\eta a$. To mimic a semi-infinite system, we use periodic boundary conditions for the xx component of the mobility tensor $\boldsymbol{\mu}_{ij}$ (implemented by the Lekner−Sperb method[23]) and consider $M = 4$ polymers with $N = 10$ monomers each grafted regularly on a square of length L. The grafting density is defined as $\rho = Ml^2/L^2$.

In our LB simulations we graft $M = 16$ semiflexible polymers on a solid surface that is constructed by a square lattice of Lennard-Jones beads. We use the 18-velocity model (D3Q18)[24] where the monomers are coupled to the solvent via a viscous damping and a white noise satisfying the standard fluctuation dissipation theorem. This method was shown to correctly reproduce hydrodynamic interactions as well as polymer motion in a viscous fluid; details are described elsewhere.[25] As will be shown, the agreement between both methods is perfect, demonstrating their equivalence within the parameter range of interest.

In Figure 1 we show representative snapshots from BD simulations for flexible $l_p/l = 0.2$ (bottom) and stiff $l_p/l = 10$ (top) chains at intermediate density $\rho = 1$ where the applied shear strength is increased as one goes from left to right. One clearly sees the chains bending toward the surface for large shear rate, which suggests that the flow stagnation layer moves toward the surface.

We now introduce our analytic mean-field method which treats a single semiflexible chain in its most likely configuration, the ground state, and subject to the hydrodynamic drag due to the mean solvent velocity profile that results from the screening of the imposed shear due to all other chains. Such a mean-field approach makes sense since hydrodynamic interactions are quite long ranged and indeed describes our numerical results for stiff enough chains and not too large shear rates very well. We regard the filament to lie in the xz plane and describe its shape by the angle $\theta(s)$ between the local tangent and the z-axis, defined along the contour s ($0 < s < l$). The potential-of-mean-force functional of the semiflexible chain consists of the bending energy and the work done by the solvent flow $u(z)$ at a distance z from the surface

$$E[\theta, u] = \int_0^l \mathrm{d}s\left[\frac{\kappa}{2}\dot{\theta}^2(s) - \zeta u(z(s))x(s)\right] \qquad (2)$$

where $x(s) = \int_0^s \mathrm{d}s' \sin\theta(s')$ and $z(s) = \int_0^s \mathrm{d}s' \cos\theta(s')$ determine the chain shape and $\zeta = 3\pi\eta$ is the friction coefficient per unit length. In our notation, $\dot{\theta}(s) = \mathrm{d}\theta/\mathrm{d}s$. Steric interactions between polymers are neglected. The Stokes equation relates the curvature of the fluid velocity $u(z)$ to the drag force exerted on the filaments

$$\eta\frac{\mathrm{d}^2}{\mathrm{d}z^2}u(z) = \zeta\rho l^{-2}\frac{u(z)}{\cos\theta(z)} \qquad (3)$$

which is similar to the Brinkman equation for flow in porous media.[26] The penetration of shear flow into a polymer brush was first studied by Milner,[8] who invoked the Brinkman equation but assumed that the brush structure is undistorted by the flow, leading to a hydrodynamic drag dependent only on the equilibrium local density. Via the term inversely proportional to $\cos\theta(z)$ in eq 3, our formulation explicitly incorporates the coupling between flow-induced deformation of semiflexible chains and modified hydrodynamic screening. Note that the flow profile $u(z)$ in eq 3 is understood as the laterally averaged flow profile; in that case the relation becomes exact as can be shown using the Stokes Green's function close to a no-slip surface.[23]

The boundary conditions are $u(z)|_{z=0} = 0$ at the grafting surface and $u'(z)|_{z=H} = \mathrm{d}u/\mathrm{d}z|_{z=H} = \dot{\gamma}$ at the free polymer end, where H denotes the normal distance of the chain end from the surface. Note that the main approximation lies in using the mean velocity profile $u(z)$ in eq 2 and in the neglect of polymer fluctuations. To minimize the functional $E[\theta,u]$ we take a derivative with respect to $\theta(s)$ leading to

$$\kappa\ddot{\theta}(s) = -\zeta \cos\theta(s) \int_s^l \mathrm{d}s'\, u(s') \tag{4}$$

with boundary conditions $\theta(s)|_{s=0} = 0$ and $\dot{\theta}(s)|_{s=l} = 0$. The Stokes equation, eq 3, can be reparameterized as

$$\ddot{u}(s) \cos\theta(s) + \dot{u}(s)\dot{\theta}(s) \sin\theta(s) = \frac{\zeta\rho}{\eta l^2} u(s) \cos^2\theta(s) \tag{5}$$

These equations are to be solved self-consistently for the polymer shape $\theta(s)$ and solvent velocity profile $u(s)$, which poses a formidable problem.

In the first approach, we assume $\theta(s) \ll 1$ and linearize the eqs 4 and 5, leading to

$$\kappa\ddot{\theta}(s) = -\zeta \int_s^l \mathrm{d}s'\, u(s') \tag{6}$$

$$\ddot{u}(s) = \frac{\zeta\rho}{\eta l^2} u(s) \tag{7}$$

These equations can be easily solved and give

$$u(s) = \xi \sinh(\lambda s) \tag{8}$$

and

$$\theta(s) = \frac{\zeta\xi}{\kappa\lambda}\left\{\frac{1}{\lambda^2}[\cosh(\lambda s) - 1] - \frac{s^2}{2}\cosh(\lambda l) + \frac{s}{\lambda}[\lambda l \cosh(\lambda l) - \sinh(\lambda l)]\right\} \tag{9}$$

with $\lambda^2 = \zeta\rho/\eta l^2$ and $\xi = \dot{\gamma}/\lambda \cosh(\lambda l)$. As can be seen in eq 7, the solvent velocity profile $u(s)$ is decoupled from the chain conformation represented by $\theta(s)$ for small $\theta \ll 1$. It is therefore expected that the linear analysis would be valid only for slightly deformed polymer brushes, i.e., at very low shear rates or at very stiff chains.

The second approach we propose for solving eqs 4 and 5 is variational: we assume the shape of the semiflexible polymer to consist of a circular section at the surface (region I: $0 < z < \tilde{H}$) and a straight segment at the free end (region II: $\tilde{H} < z < H$); see inset of Figure 2a. The filament shape is then completely specified by two variational parameters, namely the curvature, $1/R$, of the circular section and the angle, θ_0, that the straight segment makes with respect to the z-axis. The energy functional is thus expressed as

$$E(R,\theta_0) = \frac{\kappa}{2}\frac{\theta_0}{R} - \zeta\int_0^{\tilde{H}} \mathrm{d}z\, \frac{u_{\mathrm{I}}(z)x_{\mathrm{I}}(z)}{\sqrt{1 - z^2/R^2}} - \zeta\int_{\tilde{H}}^{H} \mathrm{d}z\, \frac{u_{\mathrm{II}}(z)x_{\mathrm{II}}(z)}{\cos\theta_0} \tag{10}$$

where $\tilde{H} = R \sin\theta_0$ and $H = R \sin\theta_0 + (l - R\theta_0)\cos\theta_0$. Given R and θ_0, the Stokes equation (3) can be solved for the flow profile $u(z)$ in the two regions. Minimizing $E(R,\theta_0)$ gives optimal values for R^* and θ_0^* and thus an estimate for the polymer shape and the flow profile. The fluid velocity profile and chain conformation are now coupled to one another, and this variational analysis is thus anticipated to give better estimations than the linear analysis for large shear rates.

Figure 2a shows the laterally averaged stagnated flow profile $\tilde{u}(z) = u(z)/\dot{\gamma}l$ from BD simulations (symbols), linear theory (broken line), and variational theory (solid line). Within the BD

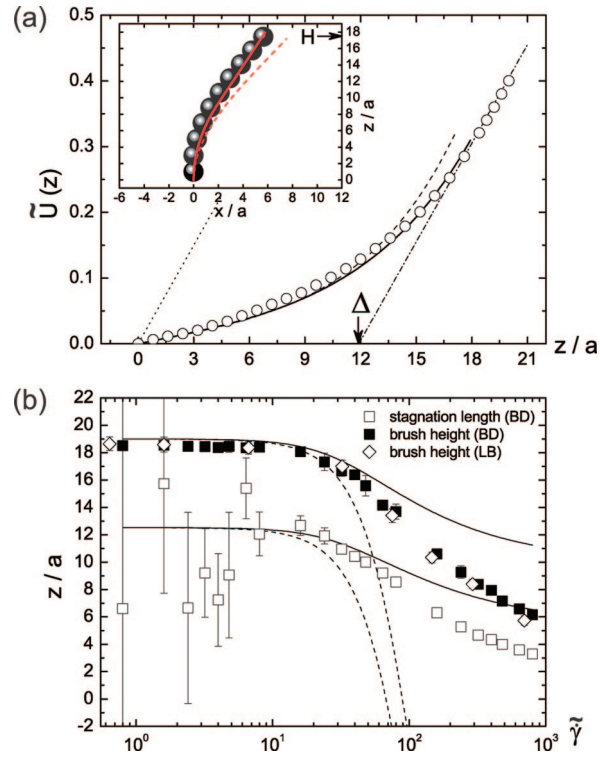

Figure 2. (a) Solvent flow profile from BD simulations (circles), compared with the prediction from variational (solid line) and linearization (broken line) analysis. The dot-dashed line shows the linear extrapolation of flow profile at the free end to extract the stagnation length. For comparison, the unperturbed flow profile in the absence of grafted chains is denoted by a dotted line. The parameters are $\rho = 1$, $l_p/l = 10$, and and $\tilde{\gamma} = 24$. The inset shows the averaged polymer configuration from BD simulations compared with variational and linear theory (solid and broken lines). (b) Stagnation length Δ from BD simulations and brush height H from BD and LB simulations vs shear strength at fixed $\rho = 1$ and $l_p/l = 10$. Predictions for H and Δ from variational theory are denoted by full lines and those from linearization theory by dashed lines.

simulations flow profiles are calculated using the laterally averaged Green's function $\bar{G}(z,z') = (z + z' - |z - z'|)/2\eta$[23] as

$$u(z) = \dot{\gamma}z - \frac{\rho}{l^2}\sum_i \bar{G}(z,z_i)\nabla_{\mathbf{r}_i} V \tag{11}$$

The inset displays the corresponding averaged polymer conformation obtained from the various approaches. The solvent velocity follows the imposed linear shear profile above the free end of chain, $\mathrm{d}u(z)/\mathrm{d}z = \dot{\gamma}$. Linearly extrapolating the flow profile at the free end to zero solvent velocity (dot-dashed line) gives the shear-induced stagnation length Δ which is a measure of how much the stagnation layer is moved away from the surface due to the presence of polymers. The comparison shows that the variational theory reproduces the simulations quite accurately, less so the linear approach. It turns out that the solvent flow penetrates deeply into the layer and almost all monomers are exposed to the flow. Depicted in Figure 2b are the brush height H and the stagnation length Δ as a function of applied shear strength for fixed grafting density $\rho = 1$ and persistence length $l_p/l = 10$. In the simulation the brush height H is obtained as the average over the positions of the terminal monomers. The variational scheme fits the simulation data quite well for not too high shear rates and in particular describes the stagnation height well for low shear rates where the simulation results are noisy. Note the excellent agreement between BD and LB simulations. Shear effects on the polymer brush heights have been controversial. Previous theoretical studies have predicted

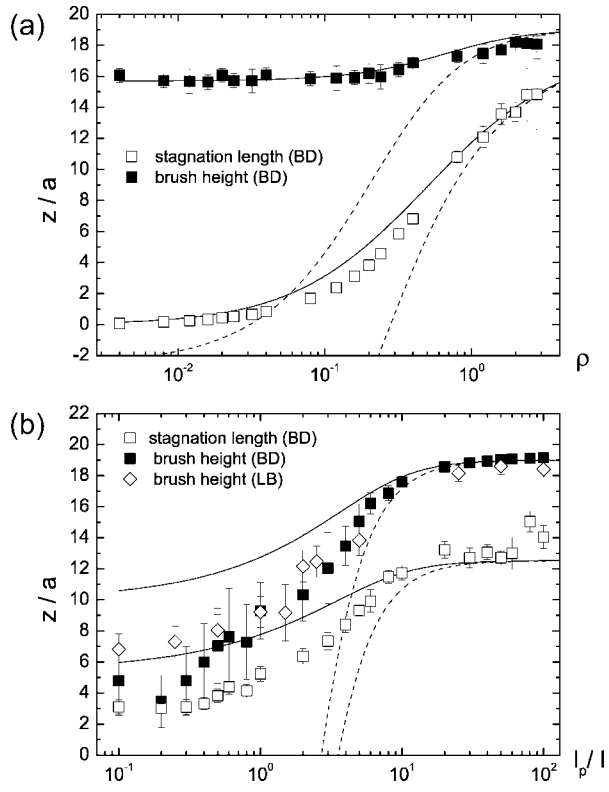

Figure 3. (a) Stagnation length and brush height vs the grafting density ρ at $\tilde{\gamma} = 24$ and $l_p/l = 10$. (b) Stagnation length and brush height vs the persistence length l_p/l at at $\tilde{\gamma} = 24$ and $\rho = 1$. Lines are defined as in Figure 2b.

swelling of flexible polymer brush layer, i.e., shear-induced thickening,[9,10] while various numerical studies have reported little change[11−13] or decrease in brush thickness at strong shear flows, i.e., shear-induced thinning.[14,15] In previous analytic approaches, the solvent flow inside the brush was not considered, and the monomer density profile has been treated in an approximate way based on the Alexander model. Numerical studies apart from molecular dynamic simulations treat the flow profile inside the layer approximately by solving the Brinkman equation.[11,14] On the other hand, the simulation methods presented here explicitly include the hydrodynamic interactions among grafted polymers. Consistent with experimental[7] and numerical observations,[11,12,14,15] our analytic and numerical results demonstrate that the brush height is not affected by weak shear, but decreases at high shear rates, supporting the shear-induced thinning scenario for the case of semiflexible polymer brushes. We note that it is difficult to directly compare our results to MD simulations with explicit solvent. This is so because those simulations typically deal with quite concentrated systems and employ strong shear flows for efficiency reasons. For example, in the MD simulation by Grest,[13] the grafting density in our notation was $\rho \sim O(10^2)$ and the applied shear rate of the order of $\tilde{\gamma} \sim O(10^3)$. More importantly, those MD simulations considered flexible polymers, whereas our model considers semiflexible polymers which makes the ground-state assumption quite accurate.

The Weissenberg number Wi characterizing the strength of shear flow acting on a soft object is defined as $Wi = \tau_r\dot{\gamma}$. Using the relaxation time of a semiflexible filament given as $\tau_r \sim \eta l^4/k_BTl_p$,[27] the Weissenberg number is directly related to the dimensionless shear rate $\tilde{\gamma} = l^3\dot{\eta}\gamma/k_BT$ via $Wi \sim \tilde{\gamma}\ l/l_p$. From Figures 2b and 3b we deduce that the brush layers begin to deform around values of $Wi \sim O(1)$.

In Figure 3a, we show the effect of the polymer grafting density ρ. In the dilute regime, the brush height is constant and the stagnation height is essentially zero, meaning that the mean solvent flow is not perturbed at all by the presence of grafted polymers. For increasing polymer density the stagnation height increases dramatically and the brush height only slightly increases due to hydrodynamic flow screening inside the brush. The behavior is correctly captured by the variational analysis: within the variational approach, the stagnation length is in general given as

$$\Delta = H - (\cos^{1/2}\theta_0/\lambda)\tanh(\lambda H/\cos^{1/2}\theta_0) \tag{12}$$

It can be shown in the limit of $\rho \to 0$ that the energy functional $E[R,\theta_0]$ becomes no longer dependent on the grafting density. Consequently, R^* and θ_0^* are independent of ρ, so is H for very dilute systems. The stagnation length then has a linear dependence on the grafting density

$$\Delta \sim \frac{3\pi\rho H^3}{l^2\cos\theta_0^*} \sim \rho \tag{13}$$

for vanishing ρ, as consistent with the simulations. Using molecular dynamic simulations, Adiga and Brenner recently studied the solvent permeability through a polymer-grafted nanopore.[5] Via solvent-induced polymer conformation changes between extended and collapsed states, a smart flow gating mechanism was proposed. They also found that the solvent permeability correlates very well with changes in the brush height. However, according to Figure 3a, this is not always true. Without significant changes in the brush height, permeability can be drastically varied by adjusting the grafting density: a brush that is perfectly permeable in the dilute regime can become effectively nondraining by increasing the grafting density of stiff chains, while the brush height remains almost unaffected. The nonlinear response of the stagnation length as a function of the grafting density can be also used for designing nanofluidic biomolecule sorting devices with two-dimensional arrays of posts.[28] The efficiency of these devices would be in principle related to the flow rates passing through molecular sieves (roughly proportional to $1/\Delta$) and the density of arrays for filtration (corresponding to ρ). It is therefore envisioned that the optimal performances of devices can be achieved at an intermediate grafting density due to the nonlinear response of the stagnation length.

In Figure 3b we present data for varying persistence length. As seen, flexible chains show smaller brush and stagnation heights which results from a combination of shape fluctuations and an enhanced susceptibility to shear. According to linear analysis, the brush and stagnation heights show a quadratic dependence on the ratio of shear strength and persistence length as

$$H = l - \frac{\tilde{\gamma}^2 l^3}{(3\pi)^{5/2} l_p{}^2 \rho^{9/2}} g(\sqrt{3\pi\rho}) \tag{14}$$

$$\Delta = H - \frac{l}{(3\pi\rho)^{1/2}}\tanh(\sqrt{3\pi\rho}) \tag{15}$$

where $g(x) = \int_0^x ds(\cosh s + A(x)s - B(x)s^2 - 1)^2/\cosh^2 x$ and $A(x) = x\cosh x - \sinh x$ and $B(x) = (\cosh x)/2$. These results are accurate for small shear in Figure 2b and large persistence length l_p/l in Figure 3b. It is interesting to note that in the linear regime the difference between H and Δ depends only on the grafting density ρ and chain length l (and not on the shear rate or persistence length, in approximate agreement with the simulation data in Figures 2b and 3b).

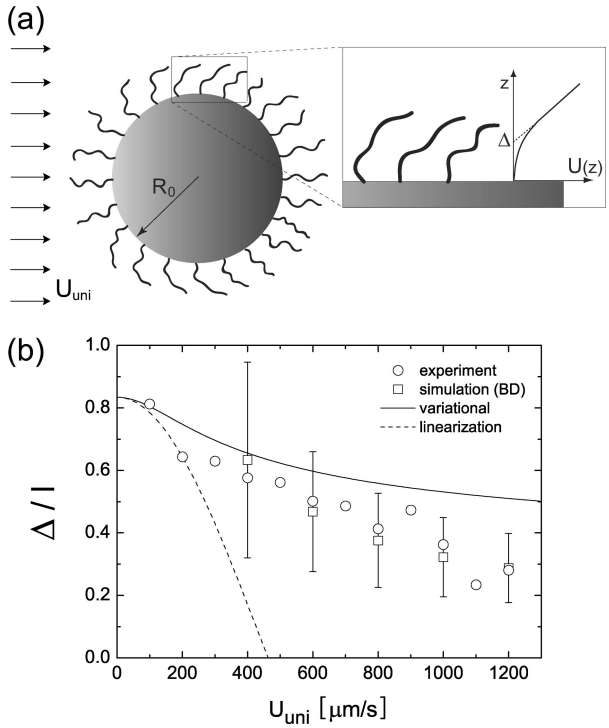

Figure 4. (a) Schematic experimental setup for a DNA-grafted colloid of radius R_0 in laminar flow of velocity U_{uni}. The inset shows the deformed DNA layer and the stagnated flow profile $U(z)$ inside the DNA brush. The stagnation length Δ is determined by linear extrapolation of $U(z)$. (b) Rescaled stagnation length Δ/l in a brush layer along the meridian perpendicular to the direction of the externally imposed flow for a DNA-grafted colloid. The parameters used in the theory and simuations are polymer length $l = 0.34$ μm, persistence length $l_p = 50$ nm, and rescaled grafting density $\rho = 3.85$. A uniform flow velocity $U_{uni} = 1000$ μm/s in the experiment corresponds to a dimensionless shear rate $\tilde{\dot{\gamma}} = 6.47$ at the meridian.

Recently, Gutsche et al. measured the drag force F on a spherical colloid of radius R_0 covered with a layer of grafted DNA in laminar flows using optical tweezers (Figure 4a).[21] The measured drag force enables us to estimate the effective hydrodynamic radius of the colloid, arising from the stagnation length under flow, with which our results can be compared as follows. Grafted chains experience the highest shear along the meridian perpendicular to the flow direction and thus the DNA/colloid complex deforms into an eliposoidal shape. For a prolate[29] the drag force in laminar flow of velocity U_{uni} is

$$F = \frac{8\pi\eta c U_{uni}}{(\tau_0^2 + 1)\coth^{-1}\tau_0 - \tau_0} \tag{16}$$

where α and β are the semimajor and minor axis lengths, $c = (\alpha^2 - \beta^2)^{1/2}$, and $\tau_0 = \alpha/c$. For slight asphericity this simplifies to $F = 6\pi\eta\beta U_{uni}(1 + \epsilon/5)$ where $\alpha = \beta(1 + \epsilon)$. Assuming the major radius to be unperturbed, $\alpha = R_0 + l$ (i.e., colloid radius plus unperturbed brush height), and the minor radius to be given by $\beta = R_0 + \Delta$ (i.e., colloid radius plus stagnation length), we obtain

$$\frac{\Delta}{l} = \frac{5}{4}\left(\frac{F}{6\pi\eta l U_{uni}} - \frac{R_0}{l} - \frac{1}{5}\right) \tag{17}$$

which thus allows to extract the stagnation length Δ from the experimentally measured drag force F. Figure 4b shows the experimental ratio of stagnation length divided by polymer length, Δ/l (circles), using a contour length $l = 0.34$ μm for 1000 bp DNA chains, and a colloid radius $R_0 = 1.1$ μm with a grafting density of 1/0.03 μm^2, leading to a rescaled density $\rho = 3.85$. In contrast to previous theoretical studies,[9,10] the stagnation length decreases with the applied flow velocity U_{uni}. This is in fair agreement with our variational theory (solid line) for which the shear rate is taken as the Stokes result for a steadily translating sphere, yielding $\dot{\gamma} = 3U_{uni}/4R_0$; in the comparison, a persistence length of $l_p = 50$ nm is used, which is the standard value expected for the experimental salt concentration of 150 mM NaCl. It is remarkable that our relatively simple analytic theory shows an excellent agreement with the experiment for very small U_{uni} (=100 μm/s). This implies that hydrodynamic mean-field theory provides a valuable tool to predict the effective hydrodynamic radius of polymer-tethered colloids in the situations of small Weissenberg number which are frequently encountered in practical applications but hard to be tackled by simulation methods. Disagreement sets in at about $U_{uni} \sim 1000$ μm/s corresponding to a shear rate of $\dot{\gamma} \sim 10^3$/s. The theory overestimates the stagnation height as expected, since $l_p/l < 1$ and chain shape fluctuations which are ignored in our analytic model are important in the regime of small l_p/l (compare Figure 3b). The simulations (squares) of a system of $M = 4$ grafted wormlike chains at grafting density $\rho = 3.85$ and persistence length $l_p = 50$ nm and length $l = 340$ nm, modeled as a string of $N = 34$ beads, give a more realistic estimate at larger flow velocities and, on the other hand, are plagued by large statistical errors for small U_{uni}. Overall, we consider the agreement between variational theory, hydrodynamic theory, and experiments very satisfactory.

In summary, we have studied grafted semiflexible chains in shear using different simulation and analytical methods and focused on the interplay between hydrodynamic screening of the solvent flow and the flow-induced chain bending. As a nontrivial test of the equivalence of different hydrodynamic numerical methods, BD and LB simulations have been performed for identical parameters values and show an excellent agreement for the investigated parameter range. It turns out that our hydrodynamic mean-field theory correlates very well with the simulations for stiff enough chains and/or not too strong shear. Therefore, in dilute systems with low applied shear rates, where numerical methods are computationally expensive, this continuum hydrodynamic mean-field theory can be very useful to design nanofluidic devices with semiflexible-grafted chains. Excellent agreement for the flow-induced nonlinear reduction of the stagnation layer height with recent streaming experiments on DNA brushes is found, lending further credibility to our hydrodynamic mean-field formalism and simulations.

Acknowledgment. Funding is acknowledged from the DFG via SPP 1164 (Nano- and Microfluidics) and via the Excellence Cluster Nano-Initiative Munich and from the Elitenetzwerk Bayern in the framework of CompInt. Y.W.K. and P.P. acknowledge support from NSF under Grants DMR 05-03347 and DMR 07-10521.

References and Notes

(1) (a) Napper, D. H. *Polymeric Stabilization of Colloidal Dispersions*; Academic: London, 1983. (b) Inn, Y.; Wang, S.-Q. *Phys. Rev. Lett.* **1996**, *76*, 467.
(2) Maroudas, A. In *Lubrication and Wear in Joint*; Wright, V., Ed.; Sector: London, 1969.
(3) Kim, Y. W.; Netz, R. R. *Phys. Rev. Lett.* **2006**, *96*, 158101.
(4) Stone, H. A.; Stroock, A. D.; Ajdari, A. *Annu. Rev. Fluid Mech.* **2004**, *36*, 381.
(5) Adiga, S. P.; Brenner, D. W. *Nano Lett.* **2005**, *5*, 2509.
(6) (a) Klein, J.; Perahia, D.; Warburg, S. *Nature (London)* **1991**, *352*, 143. (b) Klein, J. *Nature (London)* **1994**, *370*, 634.
(7) (a) Baker, S. M. *Macromolecules* **2000**, *33*, 1120. (b) Ivkov, R.; Butler, P. D.; Satija, S. K.; Fetters, L. J. *Langmuir* **2001**, *17*, 2999. (c) Anastassopoulos, D. L.; Spiliopoulos, N.; Vradis, A. A.; Toprakcioglu, C.; Baker, S. M.; Menelle, A. *Macromolecules* **2006**, *39*, 8901.
(8) Milner, S. T. *Macromolecules* **1991**, *24*, 3704.

(9) (a) Barrat, J.-L. *Macromolecules* **1992**, *25*, 832. (b) Kumaran, V. *Macromolecules* **1993**, *26*, 2464.
(10) (a) Harden, J. L.; Cates, M. E. *Phys. Rev. E* **1996**, *53*, 3782. (b) Aubouy, M.; Harden, J. L.; Cates, M. E. *J. Phys. II* **1996**, *6*, 969. (c) Sevick, E. M.; Williams, D. R. M. *Macromolecules* **1994**, *27*, 5285.
(11) (a) Lai, P. Y.; Binder, K. *J. Chem. Phys.* **1993**, *98*, 2366. (b) Miao, L.; Guo, H.; Zuckermann, M. J. *Macromolecules* **1996**, *29*, 2289.
(12) (a) Grest, G. S. *Phys. Rev. Lett.* **1996**, *76*, 4979. (b) *J. Chem. Phys.* **1996**, *105*, 5532.
(13) Grest, G. S. *Adv. Polym. Sci.* **1999**, *138*, 149.
(14) (a) Doyle, P. S.; Shaqfeh, E. S. G.; Gast, A. P. *Phys. Rev. Lett.* **1997**, *78*, 1182. (b) *Macromolecules* **1998**, *31*, 5474. (c) Saphiannikova, M. G.; Pryamitsyn, V. A.; Cosgrove, T. *Macromolecules* **1998**, *31*, 6662.
(15) (a) Peters, G. H.; Tildesley, D. J. *Phys. Rev. E* **1995**, *52*, 1882. (b) Kreer, T.; Binder, K.; Müser, M. H. *Langmuir* **2003**, *19*, 7551. (c) Huang, J.; Wang, Y.; Laradji, M. *Macromolecules* **2006**, *39*, 5546. (d) Irfachsyad, D.; Tildesley, D.; Malfreyt, P. *Phys. Chem. Chem. Phys.* **2002**, *4*, 3008.
(16) (a) Wijmans, C. M.; Smit, B. *Macromolecules* **2002**, *35*, 7138. (b) Pastorino, C.; Binder, K.; Kreer, T.; Müller, M. *J. Chem. Phys.* **2006**, *124*, 064902. (c) Müller, M.; Pastorino, C. *Europhys. Lett.* **2008**, *81*, 28002.
(17) Linden, S. K.; Sutton, P.; Karlsson, N. G.; Korolik, V.; McGuckin, M. A. *Mucosal Immunol.* **2008**, *1*, 183.
(18) Matsui, H. *Proc. Natl. Acad. Sci. U.S.A.* **2006**, *103*, 18131.
(19) (a) Ribbeck, K.; Gorlich, D. *EMBO J.* **2001**, *20*, 1320. (b) *EMBO J.* **2002**, *21*, 2664.
(20) Rant, U.; Arinaga, K.; Tornow, M.; Kim, Y. W.; Netz, R. R.; Fujita, S.; Yokoyama, N.; Abstreiter, G. *Biophys. J.* **2006**, *90*, 3666.
(21) Gutsche, C.; Salomo, M.; Kim, Y. W.; Netz, R. R.; Kremer, F. *Microfluid. Nanofluid.* **2006**, *2*, 381.
(22) (a) Schlagberger, X.; Netz, R. R. *Europhys. Lett.* **2005**, *70*, 129. (b) *Europhys. Lett.* **2005**, *70*, 563.
(23) (a) Kim, Y. W.; Netz, R. R. *Europhys. Lett.* **2005**, *72*, 837. (b) *J. Chem. Phys.* **2006**, *124*, 114709.
(24) Ladd, A. J. C. *Phys. Rev. Lett.* **1993**, *70*, 1339.
(25) (a) Ahlrichs, P.; Dünweg, B. *Int. J. Mod. Phys. C* **1998**, *9*, 1429. (b) Lobaskin, V.; Dünweg, B. *New J. Phys.* **2004**, *6*, 54.
(26) Brinkman, H. *Appl. Sci. Res. A1* **1947**, 27.
(27) Granek, R. *J. Phys. II* **1997**, *7*, 1761.
(28) (a) Volkmuth, W. D.; Austin, R. H. *Nature (London)* **1992**, *358*, 600. (b) Volkmuth, W. D.; Duke, T.; Wu, M. C.; Austin, R. H. *Phys. Rev. Lett.* **1994**, *72*, 2117. (c) Chou, C.-F. *Proc. Natl. Acad. Sci. U.S.A.* **1999**, *96*, 13762.
(29) Happel, J.; Brenner, H. *Low Reynolds Number Hydrodynamics*; Kluwer: Dordrecht, 1991.

MA900184E